Experimental Full Duplex Simultaneous Transmission of LTE Over a DWDM Directly Modulated RoF System

Thavamaran Kanesan, Wai Pang Ng, Zabih Ghassemlooy, and Chao Lu

***Abstract*—In this paper, we experimentally demonstrate the seamless integration of full duplex system frequency division duplex (FDD) long-term evolution (LTE) technology with radio over fiber (RoF) for eNodeB (eNB) coverage extension. LTE is composed of quadrature phase-shift keying (QPSK), 16-quadrature amplitude modulation (16-QAM) and 64-QAM, modulated onto orthogonal frequency division multiplexing (OFDM) and single-carrier-frequency division multiplexing for downlink (DL) and uplink (UL) transmissions, respectively. The RoF system is composed of dedicated directly modulated lasers for DL and UL with dense wavelength division multiplexing (DWDM) for instantaneous connections and for Rayleigh backscattering and nonlinear interference mitigation. DL and UL signals have varying carrier frequencies and are categorized as broad frequency spacing (BFS), intermediate frequency spacing (IFS), and narrow frequency spacing (NFS). The adjacent channel leakage ratio (ACLR) for DL and UL with 64-QAM are similar for all frequency spacings while cross talk is observed for NFS. For the best case scenario for DL and UL transmissions we achieve error vector magnitude (EVM) values of ~2.30%, ~2.33%, and ~2.39% for QPSK, 16-QAM, and 64-QAM, respectively, while for the worst case scenario with a NFS EVM is increased by 0.40% for all schemes.**

***Index Terms*—Frequency division duplex; Full duplex; Long term evolution; OFDM; Radio-over-fiber; Relay node.**

I. Introduction

Due to the exponentially growing demand of mobile broadband end users, the 3rd Generation Partnership Project (3GPP) has introduced long-term evolution (LTE) as the next-generation standard for mobile broadband. LTE is also known as fourth-generation technology, which is capable of providing higher data rates with complex technologies [1].

Manuscript received April 30, 2013; revised September 9, 2013; accepted October 11, 2013; published December 10, 2013 (Doc. ID 189752).

T. Kanesan (e-mail: thavamaran.kanesan@ieee.org), W. P. Ng, and Z. Ghassemlooy are with the Optical Communications Research Group, Northumbria University, Newcastle-upon-Tyne NE1 8ST, UK.

T. Kanesan is now with the Aston Institute of Photonic Technologies, Aston University, Birmingham B4-7ET, UK.

C. Lu is with the Photonics Research Center, Department of Electronics and Information Engineering, Hong Kong Polytechnic University, Hung Hom, Kowloon, Hong Kong, China.

http://dx.doi.org/10.1364/JOCN.6.000008

eNodeB (eNB) is the base station for LTE, designed with integrated functionality of a radio network controller, base station controller, and radio access network, thereby making it a complex, computationally intensive, and costly structure [2]. In addition, the LTE operating carrier frequency in the urban area is 2.6 GHz, which imposes higher loss in wireless propagation and therefore limits the cell edge to about 1 km radius due to the degradation of the signal-to-noise ratio (SNR) [3]. The deterioration of SNR at the cell edge has resulted in the user equipment (UE) receiving a throughput of less than 20 Mb/s [3]; therefore, consecutive deployment of eNB at every 1 km radius in an urban area is necessary to maintain the high throughput. This increases the capital expenditure (CAPEX) as well as the operating expenditure (OPEX). A direct solution to this problem would be to extend the coverage area of eNB with relay nodes (RNs), thus lowering both CAPEX and OPEX. In the urban environment the transmission is mostly based on non-line-of-sight connectivity due to high-rise buildings. However, systems with a cell extension of 3.2 km employing a line-of-sight connectivity utilizing a radio frequency (RF) wireless interface between eNB and decode-and-forward RNs has been reported [3], which is not compatible with the urban area application with the RF wireless interface. Radio-over-fiber (RoF)-based eNB offers coverage extension up to 2.1 km with multicooperative schemes as proposed in [4]. Kanesan *et al.* and Ng *et al.* have shown theoretically [5] and experimentally [6], respectively, that a much longer coverage extension of up to 68 and 60 km, respectively, can be achieved for eNB by means of RNs (i.e., amplification and forwarding [AF]) via the RoF interface. The prior reported cell extension schemes have mainly focused on the downlink (DL) transmission in a half duplex system of LTE [1,3–5].

In [7] a full duplex LTE transmission system with the RF wireless interface based on an AF RN with an eNB coverage extension of 2 km and a throughput of 13.05 Mb/s was reported, thus demonstrating that the RF wireless interface offers an insignificant impact on the eNB coverage, as the actual LTE technology aims to deliver a throughput of 100 Mb/s.

Since the impact of RF wireless interface-based eNB coverage extension has shown small improvement, in this paper, for the first time to the best of our knowledge, we are proposing and experimentally demonstrating the seamless

1943-0620/14/010008-10$15.00/0

integration of a full duplex frequency division duplex (FDD) LTE technology with the RoF interface for eNB coverage extension. The coverage extension is based on an AF RN via a 10 km RoF link. Figure 1(a) shows the existing field deployment by 3GPP where eNB is deployed at every consecutive cell with a 1 km radius. The cells are labeled as 1, 2, and 3; the eNB is directly connected to UE within each cell. In Fig. 1(b), our proposed structure connects eNB and UE via a RN within the primary cell by employing the RoF interface. Although the adjacent cell transmission is beyond the scope of this paper, we would like to indicate that single eNB coverage can be further extended to the adjacent cell with the RoF interface. The rationale for such a strategy is to reduce the deployments of eNB, thus lowering CAPEX and OPEX, which in turn accelerates the deployment of the 3GPP LTE network.

The rest of the paper is organized as follows. Section II introduces the existing optical-fiber-based full duplex system and the associated problems. Section III explains the experimental system and its theoretical background. Section IV presents and discusses the obtained results. Finally, Section V concludes the findings of the paper.

II. Proposed Full Duplex LTE System

The conventional optical-fiber-based full duplex system delivers DL and uplink (UL) transmissions over separate dedicated optical fibers without the wavelength reuse scheme [8,9]. On the contrary, some previous research reports on dedicated fibers allocated for DL and UL with the wavelength reuse scheme [10–13]. A full duplex system with dedicated DL and UL optical fibers is the logical solution to avoid Rayleigh backscattering and optical interference as these are the major performance-limiting factors [14,15]. It is important to state that Rayleigh backscattering distortion is independent of an optical modulator but is optical fiber dependent. That is, Rayleigh backscattering not only occurs due to reflective devices but arises from material imperfection of an optical fiber [16–18]. However, using separate dedicated optical fibers would significantly increase CAPEX and OPEX.

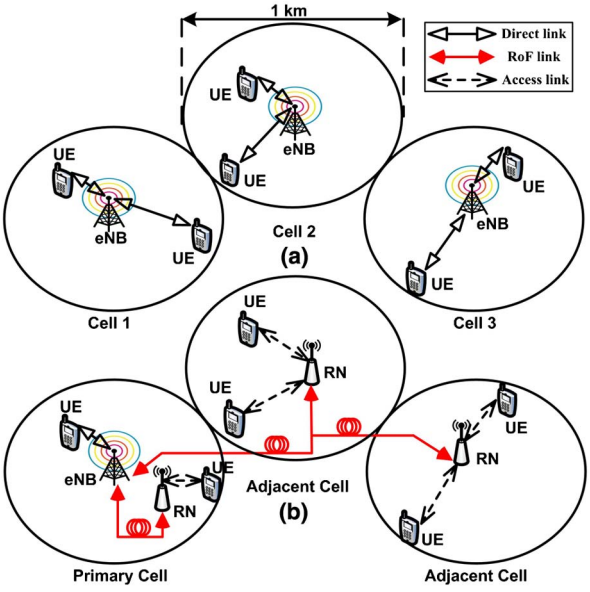

Fig. 1. Full duplex LTE radio access network structure (a) without RNs and (b) with RNs in an urban area.

In [14,19] simultaneous transmission of DL and UL signals over the same optical fiber employing wavelength reuse was reported. It is also shown in [14] that Rayleigh backscattering results in the increased noise level surrounding the vicinity of the received signal. It is also important to note that all the aforementioned optical-fiber-based full duplex systems are designed based on the external modulation scheme. In this work we have adopted a direct modulation scheme because externally modulated methods are complex and costly. However, direct modulation schemes introduce a positive frequency chirp, in contrast to externally modulated systems, which together with the chromatic dispersion degrades the system performance [20]. It is shown in [21] that the joint distortion between positive frequency chirp and chromatic dispersion introduces an average power penalty of ~3 dB. But since we are maintaining the optical launch power (OLP) within the optimum region [5], the effect of positive frequency chirp will be minimized.

In order to mitigate Rayleigh backscattering and optical interference, the proposed system is designed with two dedicated wavelengths each for UL and DL. The wavelength spacing is in the range of dense wavelength division multiplexing (DWDM) to maintain the optical spectral efficiency. In addition, having two dedicated optical carriers for both DL and UL transmission will enable instantaneous connections between eNB and UE. The system specification is designed according to the LTE requirement as stated in [22]. The full duplex system operates in the FDD mode. For the DL, carrier frequencies f_{DL} in the range of 2.62–2.69 GHz are used, whereas for the UL, upconverted carrier frequencies f_{UL} in the range of 2.5–2.57 GHz are adopted according to the LTE FDD specification [23].

In the optical layer, DL and UL signals are used to directly intensity modulate the respective distributed feedback lasers (DFBs). A direct detection scheme is employed for both DL and UL. The relevant system parameters are presented in Table I. The system evaluations for DL and UL are performed following direct detection. The evaluation is carried out both in the passband and baseband regions with the adjacent channel leakage ratio (ACLR) and the error vector magnitude (EVM), respectively.

III. Fundamentals of the Experimental System

The full duplex LTE-RoF experimental system setup is shown in Fig. 2. Fundamentals of the experimental system are as follows.

A. DL Baseband and Passband

The DL signal is generated via a vector signal generator ($\mathrm{VSG_{DL}}$; Agilent ESG E4438C). The modulated baseband

TABLE I
SYSTEM PARAMETERS

Parameters	Values
SCM modulations	QPSK, 16-QAM, and 64-QAM
Bit rate (Mb/s)	33, 66, and 100
Signal bandwidth (MHz)	20
RF power (dBm)	2 to −10
DFB bias (mA)	60
DFB bandwidth	2.7 GHz
SMF (km)	10
PD responsivity	0.42
PD bandwidth	50 GHz
LNA-gain; NF (dB)	18; 2.5

	DL	UL
MCM modulations	OFDM	SC-FDM
FFT/IFFT size	NA/2048	1024/2048
PAPR (dB)	11.16, 11.3, and 11.67	7.59, 7.71, and 7.86
Carrier frequencies (GHz)	2.62–2.69	2.5–2.57
Optical power (dBm)	1.06	1.19
Relative intensity noise (dB/Hz)	−149.6	−151.219
Optical wavelength (nm)	1551.11	1550.31

signal is in quadrature phase-shift keying (QPSK), 16-quadrature amplitude modulation (16-QAM), and 64-QAM subcarrier multiplexing (SCM) formats and can be expressed as $X_{\mathrm{DL}}(m)$, where $\{X_{\mathrm{DL}}(m): m = 0, 1, \ldots, N-1\}$, m is the subcarrier index, and N is the number of subcarriers. $X_{\mathrm{DL}}(m)$ is then modulated onto orthogonal frequency division multiplexing (OFDM) multi-carrier modulation (MCM) $S_{\mathrm{DL}}(n)$ given by [22]

$$S_{\mathrm{DL}}(n) = \frac{1}{\sqrt{N}} \sum_{m=0}^{N-1} X_{\mathrm{DL}}(m) e^{j2\pi mn/N}, \tag{1}$$

where $n = 0, 1, \ldots, N-1$ is the time domain index. The up-conversion of $S_{\mathrm{DL}}(n)$ after a digital-to-analog converter (DAC) can be described as

$$S_{\mathrm{RFDL}}(t) = \mathrm{Re}\{S_{\mathrm{DL}}(t)\} * \cos(\omega_{\mathrm{RFDL}}(t)) + \mathrm{Im}\{S_{\mathrm{DL}}(t)\} * \sin(\omega_{\mathrm{RFDL}}(t)), \tag{2}$$

$$\omega_{\mathrm{RFDL}} = 2\pi f_{\mathrm{DL}}, \tag{3}$$

where $S_{\mathrm{RFDL}}(t)$ is the passband RF OFDM signal modulated at f_{DL} ranging from 2.62 to 2.69 GHz.

B. UL Baseband and Passband

In our proposed system, the UL signal is based on single carrier-frequency division multiplexing (SC-FDM) modulation according to the LTE standard. The UL signal is realized via $\mathrm{VSG_{UL}}$ and the instrument model is consistent with the $\mathrm{VSG_{DL}}$. SC-FDM is adopted as MCM instead of OFDM in the LTE UL system. This is due to the prominent peak-to-average ratio (PAPR) problem associated with OFDM MCM. The SCM modulated signal with QPSK, 16-QAM, and 64-QAM can be expressed as $X_{\mathrm{UL}}(p)$, where $\{X_{\mathrm{UL}}(p): p = 0, 1, \ldots, M-1\}$ and p is the spreading index. $X_{\mathrm{UL}}(p)$ is transformed to the frequency domain by applying an M-point fast Fourier transform (FFT) [22]:

$$X_{\mathrm{UL}}(k) = \sum_{p=0}^{M-1} X_{\mathrm{UL}}(p) e^{-j2\pi pk/M}, \tag{4}$$

where $\{X_{\mathrm{UL}}(k): k = 0, 1, \ldots, M-1\}$ is the frequency domain SCM signal and k is the frequency domain spreading index. The M-point FFT is applied to spread the signal energy to the entire spectrum to reduce the PAPR. The contrast of the spreading can be observed from Table I in terms of PAPR values of SC-FDM and OFDM. $X_{\mathrm{UL}}(k)$ is mapped with the localized topology $X_{\mathrm{UL}}(l)$, where l is the mapping index. The localized topology for symbol mapping $\{X_{\mathrm{UL}}(l): l = 0, 1, \ldots, N-1\}$ can be described as

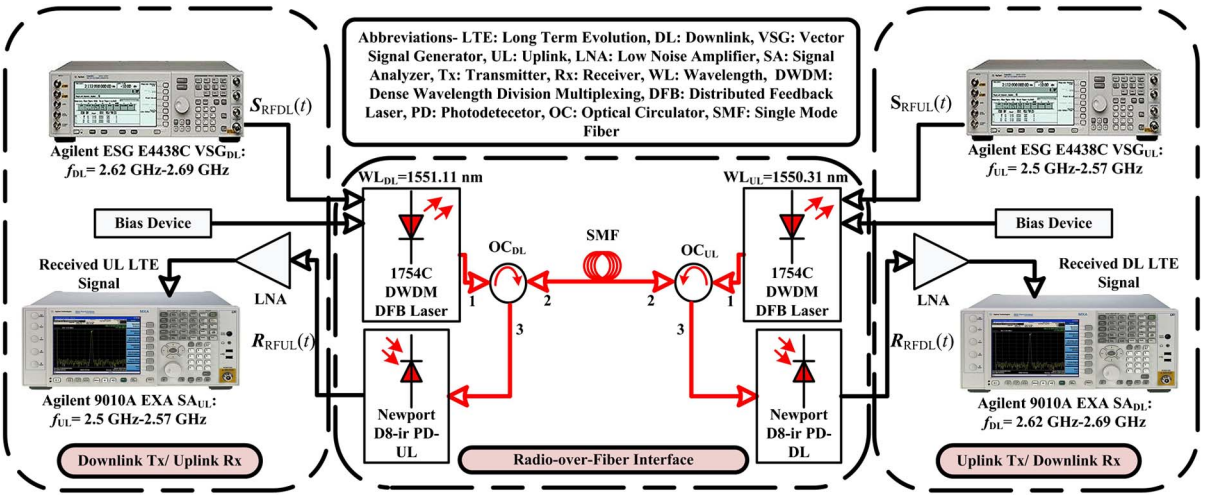

Fig. 2. Full duplex LTE experimental setup.

$$X_{\mathrm{UL}}(l) = \begin{cases} X_{\mathrm{UL}}(k), 0 \le k \le M-1 \\ 0, M \le k \le N-1 \end{cases}. \quad (5)$$

$X_{\mathrm{UL}}(l)$ is then converted to the time domain samples with N-point inverse FFT (IFFT), denoting that $N > M$:

$$S_{\mathrm{UL}}(n) = \frac{1}{N}\sum_{l=0}^{N-1} X_{\mathrm{UL}}(l) e^{j2\pi nl/N}, \quad (6)$$

where $\{S_{\mathrm{UL}}(n) : n = 0, 1, \ldots, N-1\}$ is the localized mapped SC-FDM signal in the time domain. As mentioned earlier, the PAPR of $S_{\mathrm{UL}}(n)$ is lower than that of $S_{\mathrm{DL}}(n)$. The PAPR is analytically expressed as $\mathrm{PAPR}\{S_{\mathrm{DL/UL}}(n)\} = \max\{S_{\mathrm{DL/UL}}(n)^2\}/E\{S_{\mathrm{DL/UL}}(n)^2\}$, where $E\{\cdot\}$ refers to the expectation operator.

The baseband-to-passband upconversion process is similar to that expressed in Eqs. (2) and (3). The SC-FDM signal upconversion after DAC is given by

$$S_{\mathrm{RFUL}}(t) = \mathrm{Re}\{S_{\mathrm{UL}}(t)\} * \cos(\omega_{\mathrm{RFUL}}(t)) + \mathrm{Im}\{S_{\mathrm{UL}}(t)\} * \sin(\omega_{\mathrm{RFUL}}(t)), \quad (7)$$

$$\omega_{\mathrm{RFUL}} = 2\pi f_{\mathrm{UL}}, \quad (8)$$

where $S_{\mathrm{RFUL}}(t)$ is the passband RF SC-FDM signal modulated at the f_{UL} ranging from 2.5 to 2.57 GHz.

C. Direct Modulation and DFB

This section describes direct intensity modulation of DFB lasers at wavelengths of 1551.11 and 1550.31 nm using $S_{\mathrm{RFDL}}(t)$ and $S_{\mathrm{RFUL}}(t)$, respectively. Owing to the bipolar nature of the electrical signal, a bias current is added to the signal. It is important to state that the DFB lasers are impedance matched to the operating frequencies of the proposed system. The fundamentals of intensity modulation direct detection can be defined through the laser rate equations [24].

The optical circulator for DL ($\mathrm{OC_{DL}}$) and UL ($\mathrm{OC_{UL}}$) induces an optical loss of ~3.8 and ~5.9 dB, respectively, thus resulting in OLPs of ~1.06 and ~1.19 dBm for DL and UL, respectively; see Fig. 2. These losses are due to the signal leakage from port 2 to port 3 of $\mathrm{OC_{DL}}$ and $\mathrm{OC_{UL}}$. The leakage effectively manifests itself as the cross talk and will be analyzed via ACLR measurement.

D. SMF

In this paper, the DL and UL signals at the output of port 2 of $\mathrm{OC_{DL}}$ and $\mathrm{OC_{UL}}$, respectively, are concurrently launched into 10 km of single mode fiber (SMF). The analytical model that governs the propagation properties of SMF can be expressed by the generalized nonlinear Schrödinger equation [25]. The OLPs for DL and UL are maintained within the linear propagation region to avoid nonlinear interference.

After propagating through 10 km of SMF, DL and UL signals are detected at port 3 of $\mathrm{OC_{UL}}$ and $\mathrm{OC_{DL}}$, respectively, via a Newport D8-ir photodetector (PD) with the direct detection scheme. Following photodetection, the received RF DL and UL signals are amplified via a low-noise amplifier (LNA) and subsequently demodulated using the Agilent 9020A MXA signal analyzer (SA). The demodulation is the reverse of the transmission process, except for the additional zero forcing with minimum mean square error equalizers for distortion compensation and additional noise suppression, respectively [26]. In real field deployment, the DL signal will be amplified and forwarded to an UE instead of being demodulated via SA.

IV. Results and Discussion

The full duplex LTE-FDD system operates at f_{DL} of 2.62–2.69 GHz and f_{UL} of 2.5–2.57 GHz. The DL and UL optical signal leakage in $\mathrm{OC_{DL}}$ and $\mathrm{OC_{UL}}$ will effectively interfere with the receiving UL and DL optical signals, respectively, in port 3. In principal, no interference will take place between the DL optical signal leakage and the receiving UL optical signal in $\mathrm{OC_{DL}}$, which is the same case as for the UL optical signal leakage and the receiving DL optical signal in $\mathrm{OC_{UL}}$. However, photodetection will instigate an intermodulation (IMD) product between signal leakages and the received signals for both DL and UL due to the subcarrier–subcarrier intermixing. Previously in [27] a simulation-based half duplex transmission investigation to demonstrate IMD impact on the high-frequency multiband transmission has been reported. Herein, the ACLR metric is applied to measure the IMD phenomenon in our system.

A. ACLR Measurement

The ACLR is exploited to measure the IMD between DL and UL, and it can be analytically shown as

$$\mathrm{ACLR1} = \frac{\int_{f_{\mathrm{DL/UL}}-3B/2}^{f_{\mathrm{DL/UL}}-B/2} \boldsymbol{R}_{\mathrm{RFDL/RFUL}}(f)\mathrm{d}f + \int_{f_{\mathrm{DL/UL}}+B/2}^{f_{\mathrm{DL/UL}}+3B/2} \boldsymbol{R}_{\mathrm{RFDL/RFUL}}(f)\mathrm{d}f}{\int_{f_{\mathrm{DL/UL}}-B/2}^{f_{\mathrm{DL/UL}}+B/2} \boldsymbol{R}_{\mathrm{RFDL/RFUL}}(f)\mathrm{d}f}$$

$$\mathrm{ACLR2} = \frac{\int_{f_{\mathrm{DL/UL}}-5B/2}^{f_{\mathrm{DL/UL}}-3B/2} \boldsymbol{R}_{\mathrm{RFDL/RFUL}}(f)\mathrm{d}f + \int_{f_{\mathrm{DL/UL}}+3B/2}^{f_{\mathrm{DL/UL}}+5B/2} \boldsymbol{R}_{\mathrm{RFDL/RFUL}}(f)\mathrm{d}f}{\int_{f_{\mathrm{DL/UL}}-B/2}^{f_{\mathrm{DL/UL}}+B/2} \boldsymbol{R}_{\mathrm{RFDL/RFUL}}(f)\mathrm{d}f}, \quad (9)$$

where ACLR1 and ACLR2 are the first and second adjacent band measurements. ACLR1 measures the adjacent band of 30 MHz spacing from $f_{\mathrm{DL/UL}}$, whereas ACLR2 covering the adjacent band for the 50 MHz band away from $f_{\mathrm{DL/UL}}$. This is because, in the FDD duplex scheme, the minimum spacing between f_{DL} and f_{UL} is 50 MHz for the chosen band. B is the 20 MHz signal bandwidth, $\boldsymbol{R}_{\mathrm{RFDL/RFUL}}(f)$ is the Fourier-transformed received analog signal of both

DL and UL. The integrated bandwidth of adjacent cell measurement is 20 MHz.

Figure 3 shows the half-duplex ACLR measurements of $S_{\mathrm{RFDL}}(t)$ and $S_{\mathrm{RFUL}}(t)$. $S_{\mathrm{RFDL}}(t)$ is composed of QPSK, 16-QAM, and 64-QAM with OFDM. $S_{\mathrm{RFUL}}(t)$ is modulated with the same SCMs but with SC-FDM as the MCM. The result in Fig. 3 is measured using SA after transmission over 10 km SMF with a varying RF transmit power. Herein, the RF transmit power refers to the electrical power of $S_{\mathrm{RFDL/RFUL}}(t)$. At 2 dBm RF transmit power, the average ACLR values of $S_{\mathrm{RFDL}}(t)$ and $S_{\mathrm{RFUL}}(t)$ SCMs are ~ -28.60 and ~ -28.65 dBc, respectively.

According to the LTE standard defined by [28], the ACLR requirement of LTE is −45 dBc. However, in our case, the ACLR is in the range of ~ -28 dBc as shown in Fig. 3. This is because of the responsivity of the PD used, which is 0.42 (see Table I) and the resolution bandwidth of the SA. Therefore, the detected electrical signal is close to the noise floor of SA, thus directly increasing the ACLR. This is the best achievable case in our lab using off-the-shelf components, but a lower ACLR is achievable by utilizing a PD with responsivity close to 1 to effectively increase the ACLR from ~ -28 to ~ -35.5 dBc. The intention of this paper is to demonstrate the system performance under the reasonable noise spectral density, which in this case is −114.04 dBm/Hz. Hence, we did not reduce the resolution bandwidth (150 kHz) in order to artificially produce lower noise spectral density and effectively achieve a lower ACLR. However, there are three approaches that can be adopted to achieve a lower ACLR. First, a bandpass filter can be placed right after the LNA (see Fig. 1). Since we wanted to exhibit the exact performance of the proposed system no filter is used. Second, the ACLR can be further improved by using a power amplifier cascaded with a bandpass filter. Since the ACLR is an out-of-band measurement, it does not reflect the in-band SNR. Therefore, the high gain from the power amplifier and the out-of-band attenuating characteristic of a bandpass filter can satisfy the required ACLR. Finally, the SA can be replaced with electrical receivers specifically designed for OFDM signals, as shown in [29–31], which achieved very low noise spectral density of −142.5, −155, and −154 dBm/Hz, respectively. Thus the required ACLR can be readily achieved. These options can be decided at the convenience of the system architect. Since Fig. 3 indicates that SCMs of both $S_{\mathrm{RFDL}}(t)$ and $S_{\mathrm{RFUL}}(t)$ have resulted in a similar ACLR, the rest of the ACLR analysis will be only carried out for the SCM with the highest bit rate, namely, 64-QAM in this case.

As mentioned earlier for the FDD scheme, the frequency allocations for $S_{\mathrm{RFDL}}(t)$ and $S_{\mathrm{RFUL}}(t)$ are 2.62–2.69 GHz and 2.5–2.57 GHz, respectively. As an initial step for system design, it is vital to investigate the interferences between the given frequency spacings. Figure 4 depicts the measurement recorded following photodetection for $S_{\mathrm{RFDL}}(t)$ and $S_{\mathrm{RFUL}}(t)$ at 2 dBm transmit power. In this investigation, f_{DL} swept through 2.62–2.69 GHz for a given interfering f_{UL}. The frequency spacing between $S_{\mathrm{RFDL}}(t)$ and $S_{\mathrm{RFUL}}(t)$ varies between 190 and 50 MHz. The broad frequency spacing (BFS) of 190 MHz could be achieved by transmitting at f_{DL} and f_{UL} of 2.69 and 2.5 GHz, respectively. Transmitting at f_{DL} and f_{UL} of 2.69 and 2.57 GHz, respectively, will result in 120 MHz frequency spacing denoted as the intermediate frequency spacing (IFS). Frequency spacing of 50 MHz would be the case for f_{DL} and f_{UL} of 2.62 and 2.57 GHz, respectively, which is termed the narrow frequency spacing (NFS). The details of carrier frequencies and the frequency spacing are shown in Table II.

In Fig. 4, at f_{DL} of 2.69 GHz with the interfering f_{UL} of 2.5 GHz for BFS, the ACLR is ~ -28.59 dBc. In comparison to the half-duplex system's ACLR of ~ -28.60 dBc (Fig. 3), the BFS transmission resulted in a negligible ACLR penalty. As indicated in [14], Rayleigh backscattering increases the noise level around the signal. The comparison of the full duplex system to the half duplex system's ACLR shows the proposed architecture effectively mitigates Rayleigh backscattering and other nonlinear effects altogether. Transmitting at the aforementioned f_{DL} with f_{UL} of 2.57 GHz for the IFS has resulted in an ACLR of ~ -27.91 dBc. Compared to the half-duplex system, the full duplex system with the IFS has introduced an ACLR

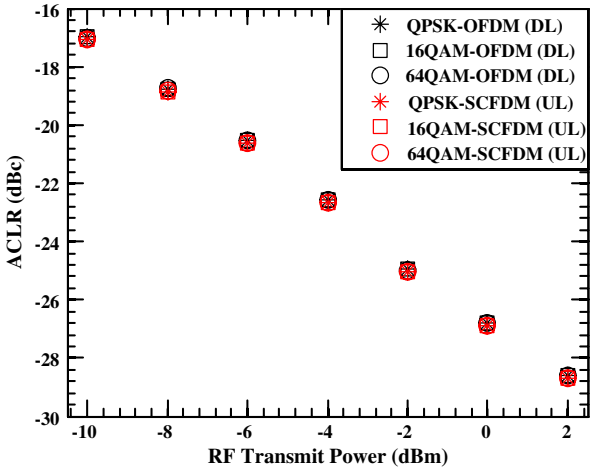

Fig. 3. ACLR for a half-duplex system of DL and UL after 10 km transmission.

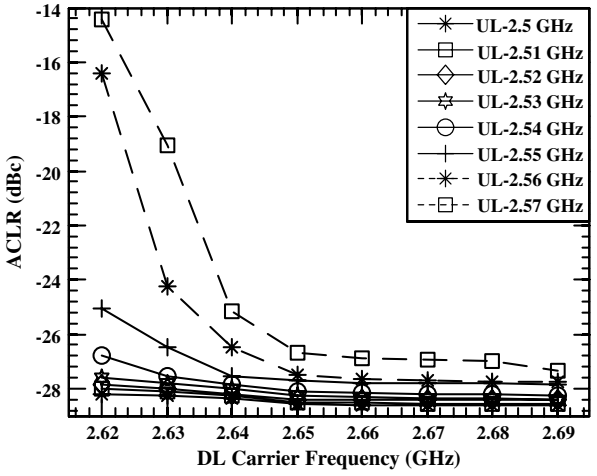

Fig. 4. ACLR of a full duplex system with DL transmission and interfering UL signal for a 64-QAM system.

TABLE II
DL AND UL FREQUENCY SPACING

f_{DL}	f_{UL}	Frequency Spacing
2.69 GHz	2.5 GHz	190 MHz (Broad)
2.69 GHz	2.57 GHz	120 MHz (Intermediate)
2.62 GHz	2.57 GHz	50 MHz (Narrow)

penalty of ~0.69 dB. Further investigation of the IFS with a shift in f_{DL} and f_{UL} to 2.62 and 2.5 GHz, respectively, attains an ACLR of ~ – 27.93 dBc. Both IFS signals result in a similar ACLR, thus demonstrating the degradation of the ACLR to be frequency spacing dependent and carrier frequency independent. Transmitting at f_{DL} of 2.62 GHz with f_{UL} of 2.57 GHz for an NFS results in a significantly higher ACLR of ~ – 14.44 dBc. The ACLR penalty for the NFS compared to the half-duplex system (Fig. 3) is ~14.16 dB. It is clear that the implication of IMD with an NFS is critical. Alternative signals that propagate within this spacing would be heavily distorted due to the IMD induced spectral regrowth. The BFS (190 MHz), IFS (120 MHz), and NFS (50 MHz) frequency spacing results in a negligible ~0.69 and an ~14.16 dB ACLR penalty, respectively, as shown in Table III.

It is necessary to indicate if the ACLR of $S_{RFUL}(t)$ would experience a similar degradation pattern with respect to the frequency spacing; hence, we carried out a homogeneous measurement as was done for $S_{RFDL}(t)$. In Fig. 5, $S_{RFUL}(t)$ and $S_{RFDL}(t)$ are transmitted at 2 dBm transmit power. f_{UL} of 2.5 GHz transmission with interfering f_{DL} of 2.69 GHz resulted in an ACLR of ~ – 28.64 dBc for BFS. Comparing the BFS ACLR of ~ – 28.64 dBc to the half-duplex system's ACLR of ~ – 28.65 dBc (Fig. 3), the ACLR penalty is negligible. Transmitting at f_{UL} of 2.57 GHz with the intercepting f_{DL} at 2.69 GHz for IFS showed an ACLR of ~ – 28.05 dBc. Compared to the half-duplex system, the IFS results in an ACLR penalty of ~0.60 dB.

At NFS with f_{UL} of 2.57 GHz and f_{DL} of 2.62 GHz transmission, the resultant ACLR is ~ – 14.53 dBc. The NFS contemplated an ACLR penalty of ~14.12 dB. The effective ACLR penalty for BFS, IFS, and NFS are negligible at ~0.60 and ~14.12 dB, respectively. Table III summarizes the ACLR penalties for the aforementioned frequency spacings. As mentioned earlier, the significant ACLR deterioration of NFS is due to the high IMD. The achieved ACLR and ACLR penalty indicate a similar degradation pattern between Figs. 4 and 5 in terms of the frequency spacing. Fundamentally, the similarity shows that the frequency spacing induced distortion is independent of MCM.

TABLE III
FREQUENCY SPACING ACLR PENALTY PRODUCT

Frequency Spacing	ACLR Penalty: $S_{RFDL}(t)$	ACLR Penalty: $S_{RFUL}(t)$
50 MHz	14.16 dB	14.12 dB
120 MHz	0.69 dB	0.6 dB
190 MHz	Negligible	Negligible

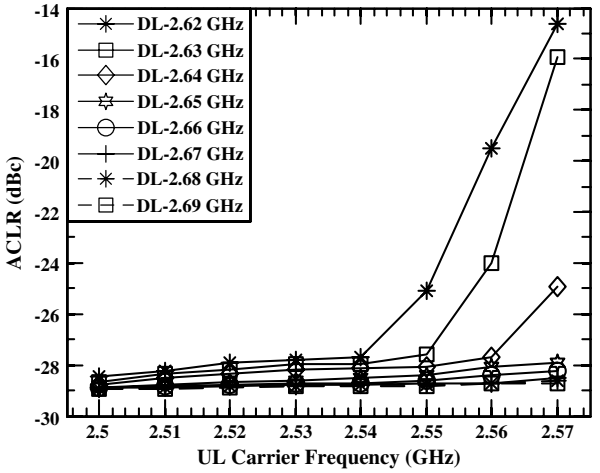

Fig. 5. ACLR of a full duplex system with UL transmission and interfering DL signal for a 64-QAM system.

B. Impact of Interfering Signal Power

In the previous section, it was shown that an NFS (50 MHz) introduced a high IMD, and an ACLR performance metric was adopted to measure the energy of IMD products. Focusing on NFS, we continue to apply the ACLR to measure the impact of interfering signals $S_{RFUL}(t)$ and $S_{RFDL}(t)$ with the varying RF transmit power level on the received $S_{RFDL}(t)$ and $S_{RFUL}(t)$, as shown in Figs. 6(a) and 6(b), respectively. $S_{RFDL}(t)$ and $S_{RFUL}(t)$ are transmitted at f_{DL} of 2.62 GHz and f_{UL} of 2.57 GHz, respectively. For Fig. 6(a), $S_{RFDL}(t)$ is transmitted at 2 dBm and the interfering $S_{RFUL}(t)$ is varied between 2 and –10 dBm, and the maximum RF transmit power is limited to 2 dBm to avoid third-order IMD in a direct modulation scenario. The response of interfering $S_{RFUL}(t)$ power variation can be observed in Fig. 7, where the RF transmit power of $S_{RFUL}(t)$ in Figs. 7(a) and 7(b) are 2 and –10 dBm, respectively, while $S_{RFDL}(t)$ is fixed at 2 dBm.

From Fig. 6(a), transmitting both $S_{RFDL}(t)$ with the interfering signal $S_{RFUL}(t)$ at 2 dBm results in an ACLR of ~ – 14.44 dBc. The resultant high ACLR is due to the IMD products as shown in Fig. 7(a). When the RF transmit power of $S_{RFUL}(t)$ is reduced to –10 dBm, the ACLR of

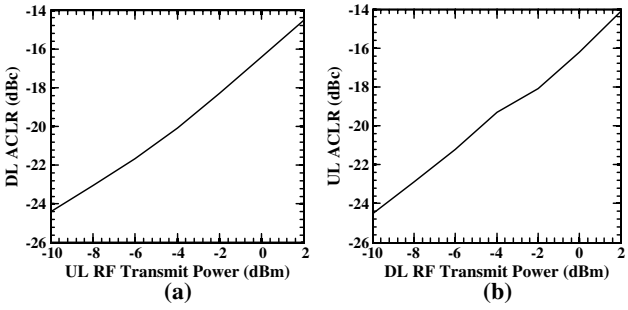

Fig. 6. ACLR of (a) DL and (b) UL with respect to the interfering UL and DL RF transmit power. DL, f_{DL} at 2.62 GHz and UL, f_{UL} at 2.57 GHz.

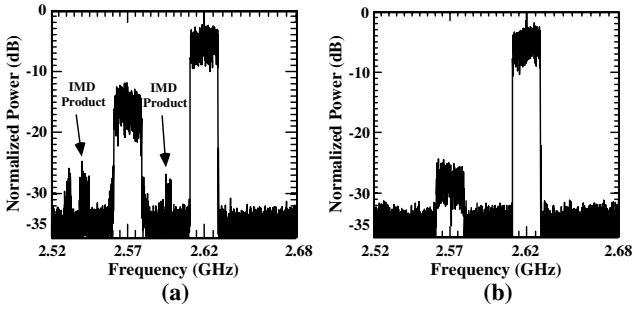

Fig. 7. Received spectral response of DL, $f_{DL} = 2.62$ GHz, and UL, $f_{UL} = 2.57$ GHz, with varying UL RF transmit power: (a) 2 dBm and (b) −10 dBm.

$S_{RFDL}(t)$ is ∼ − 24.41 dBc, thus showing an improvement of ∼9.97 dB. The outcome of this improvement can be observed in Fig. 7(b), which is relative to the suppression of IMD products. A similar investigation is carried out for $S_{RFUL}(t)$ with the interfering $S_{RFDL}(t)$ as shown in Fig. 6(b), where $S_{RFUL}(t)$ and $S_{RFDL}(t)$ are maintained at the same frequencies. This time around, $S_{RFDL}(t)$ RF transmit power is varied between 2 dBm and −10 dBm instead of $S_{RFUL}(t)$, while $S_{RFUL}(t)$ is maintained at 2 dBm. The impact of power variation of $S_{RFDL}(t)$ on $S_{RFUL}(t)$ in terms of the spectral response can be observed from Figs. 8(a) and 8(b), which depict the interfering signal of 2 and −10 dBm, respectively. The resultant ACLR observed in Fig. 6(b) for $S_{RFUL}(t)$ is ∼ − 14.53 dBc with the interfering signal transmitted at 2 dBm. This high ACLR value is due to the IMD products as shown in Fig. 8(a). Conversely, transmitting the interfering signal at −10 dBm resulted in an ACLR of ∼ − 24.53 dBc. The improvement in ACLR is associated with the IMD suppression as depicted in Fig. 8(b). From the viewpoint of the out-of-band distortion, both $S_{RFDL}(t)$ [Fig. 6(a)] and $S_{RFUL}(t)$ [Fig. 6(b)] have a similar degradation pattern relative to the interfering signal. Additionally, we found that at an NFS, the subcarrier–subcarrier intermixing due to photodetection is power dependent and can be mitigated by lowering the interfering signal power level.

However, the investigation only reveals the response of the out-of-band distortion; thus the EVM measurement is vital to further investigate the in-band distortion that can be analytically expressed as [32]

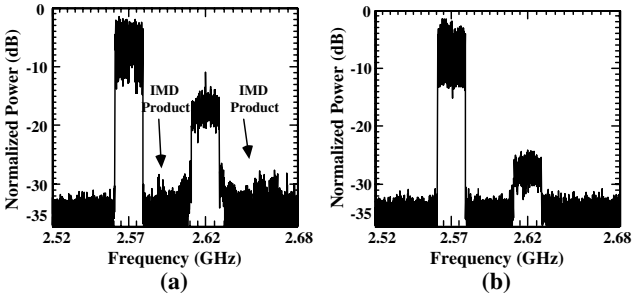

Fig. 8. Received spectral response of UL- f_{UL} 2.57 GHz and DL- f_{DL} 2.62 GHz with varying DL RF transmit power: (a) 2 dBm and (b) −10 dBm.

$$\text{EVM} = \frac{\sqrt{\frac{1}{\sqrt{N}}\sum_{n=1}^{N}|R_{DL/UL}(n) - S_{DL/UL}(n)|^2}}{R_{max}}, \quad (10)$$

where $R_{DL/UL}$ is the received baseband symbols of DL and UL, and R_{max} is the maximum magnitude of the ideal transmitted symbol utilized for normalization. In [28], the EVM requirements were 17.5%, 12.5%, and 8% for QPSK, 16-QAM, and 64-QAM, respectively. But in [33], the minimum EVM requirement has been dropped to 8% across all SCMs. Thus, the 8% EVM will be the figure of merit for the proposed system throughout the paper. It is also important to state that the ACLR requirement remains unchanged from [28].

Since the EVM metric provides explicit and precise quality of the received signal compared to the ACLR metric, the combination of RF transmit power of the received and interfering signals would provide an enhanced guideline on the basis of system design. Therefore, we are presenting multiple EVM combinations at an NFS of $S_{RFDL}(t)$ and $S_{RFUL}(t)$ with respect to the interfering $S_{RFUL}(t)$ and $S_{RFDL}(t)$, as shown in Figs. 9(a) and 9(b), respectively. The EVM is presented as a function of the color coding. $S_{RFDL}(t)$ [Fig. 9(a)] is transmitted at f_{DL} of 2.62 GHz and with a varying power of 2 to −10 dBm, while the interfering $S_{RFUL}(t)$ is transmitted at f_{UL} of 2.57 GHz with a similarly varying power. In Fig. 9(a), transmitting $S_{RFDL}(t)$ at 2 dBm

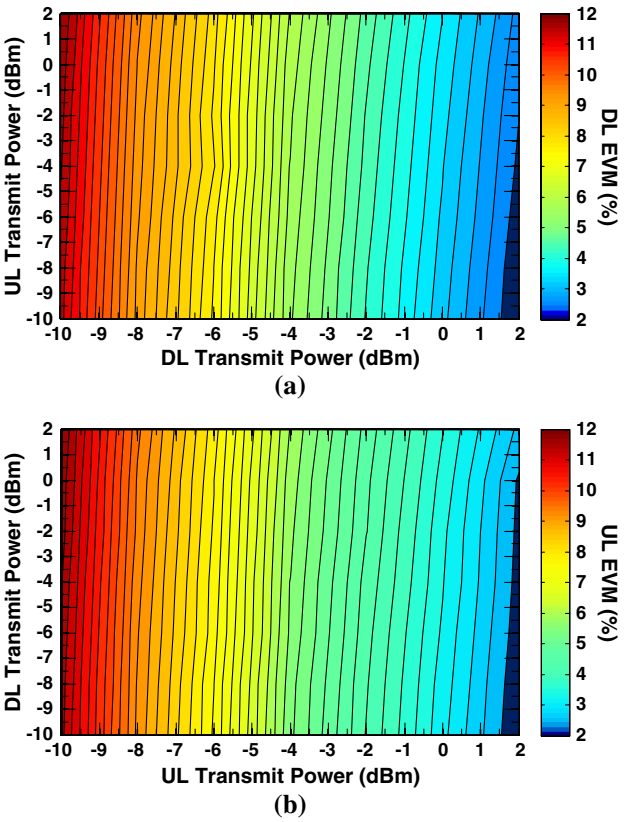

Fig. 9. Multiple EVM combinations of (a) DL and (b) UL RF transmit power with respect to the interfering UL and DL RF transmit power, respectively. DL signal is transmitted at 2.62 GHz and UL signal is transmitted at 2.57 GHz.

TABLE IV
EVM IMPACT BASED ON INTERFERING SIGNAL POWER

Interfering Signal Power	$S_{RFDL}(t)$	$S_{RFUL}(t)$
2 dBm; −10 dBm	2 dBm: ∼2.67%; ∼2.26%	2 dBm: ∼2.64%; ∼2.26%
2 dBm; −10 dBm	−10 dBm: ∼11.92%; ∼11.55%	−10 dBm: ∼11.9%; ∼11.47%

with an interfering signal $S_{RFUL}(t)$ at 2 and −10 dBm results in an EVM of ∼2.67% and ∼2.26%, respectively. At a low RF transmit power of −10 dBm for $S_{RFDL}(t)$ with an interfering signal $S_{RFUL}(t)$ at 2 and −10 dBm, the observed EVMs are ∼11.92% and ∼11.55%, respectively. The interfering signal with a lower power transmission provides an improved EVM for the received signal, which agrees well with results from the ACLR measurement. In addition, $S_{RFDL}(t)$ transmitted at < -6 dBm would not comply with the 3GPP LTE EVM limit; therefore it is essential that system designers maintain the RF transmit power level within the boundary of > -6 dBm. Multiple EVM combinations presented in Fig. 9(a) reveal that irrespective of the $S_{RFDL}(t)$ RF transmit power, the average EVM deviation is ∼0.40% when the interfering signal $S_{RFUL}(t)$ is transmitted between 2 and −10 dBm. The multiple EVM combinations are not presented for QPSK and 16-QAM systems. However, the average EVM reductions compared to the 64-QAM system are ∼0.15% and ∼0.08%, respectively, for all transmission states.

Multiple EVM combinations of the UL system are carried out by measuring $S_{RFUL}(t)$ as the receiving signal with the interfering signal $S_{RFDL}(t)$ as shown in Fig. 9(b). $S_{RFUL}(t)$ and $S_{RFDL}(t)$ are maintained at f_{UL} of 2.57 GHz and f_{DL} of 2.62 GHz, respectively, while the RF transmit power is varied between 2 and −10 dBm for both signals. The resultant EVMs are ∼2.64% and ∼2.26% for a fixed $S_{RFUL}(t)$ at 2 dBm while the interfering signal $S_{RFDL}(t)$ is transmitted at 2 and −10 dBm, respectively. For $S_{RFUL}(t)$ with a lower RF transmit power of −10 dBm, the EVMs observed with an interfering signal $S_{RFDL}(t)$ transmitted at 2 and −10 dBm are 11.90% and ∼11.47%, respectively. The EVM boundary of $S_{RFUL}(t)$ is to maintain the RF transmit power at > -6 dBm, which is the same for the case of $S_{RFDL}(t)$ [Fig. 9(a)]. The EVM deviation is ∼0.39% for $S_{RFUL}(t)$ for any RF transmit power levels with an interfering signal $S_{RFUL}(t)$ transmitted between 2 and −10 dBm, which is approximately equivalent to the EVM deviation of $S_{RFDL}(t)$. The EVM reductions for QPSK and 16-QAM of $S_{RFUL}(t)$ for multiple EVM combinations are approximately equivalent to the reduction rate of $S_{RFDL}(t)$.

The results in Figs. 9(a) and 9(b) are comprised of a linear pattern with closely related EVMs; thus, such a relationship explains that the in-band distortion induces the same impact for OFDM- and SC-FDM-based MCMs. The summary of EVMs from Figs. 9(a) and 9(b) is presented in Table IV.

C. Best Case and Worst Case Transmission Condition

As a summary of the overall system performance, the full duplex QPSK, 16-QAM, and 64-QAM SCMs are analyzed. SCMs are evaluated in terms of EVM with respect to the RF transmit power. $S_{RFDL}(t)$ and $S_{RFUL}(t)$ are classified as the best case transmission conditions with f_{DL} at 2.69 GHz and f_{UL} at 2.5 GHz (BFS). The worst case transmission condition is defined for a NFS, where $S_{RFDL}(t)$ and $S_{RFUL}(t)$ are transmitted at f_{DL} of 2.62 GHz and f_{UL} of 2.57 GHz. Figures 10(a), 10(b), and 10(c) depict QPSK, 16-QAM, and 64-QAM, respectively, for $S_{RFDL}(t)$ and $S_{RFUL}(t)$ systems. For QPSK, see Fig. 10(a); at a transmit power of 2 dBm the best case and worst case average EVMs are ∼2.30% and ∼2.54%, respectively. Inset I of Fig. 10(a) represents the constellation of QPSK at 2 dBm transmit power. The EVM is severely degraded at −10 dBm transmit power, where the best case and worst case transmission conditions resulted in ∼11.09% and ∼11.43%, respectively. Inset II shows the heavily distorted QPSK constellation at −10 dBm. Since the EVM for −10 dBm is very much higher than the LTE limit, transmission at this power is not advisable. Such profound distortion occurring at −10 dBm is due to the weak optical modulation index. The lowest transmission power that could achieve an EVM below 8% is −6 dBm, which is consistent with the finding of Subsection IV.B.

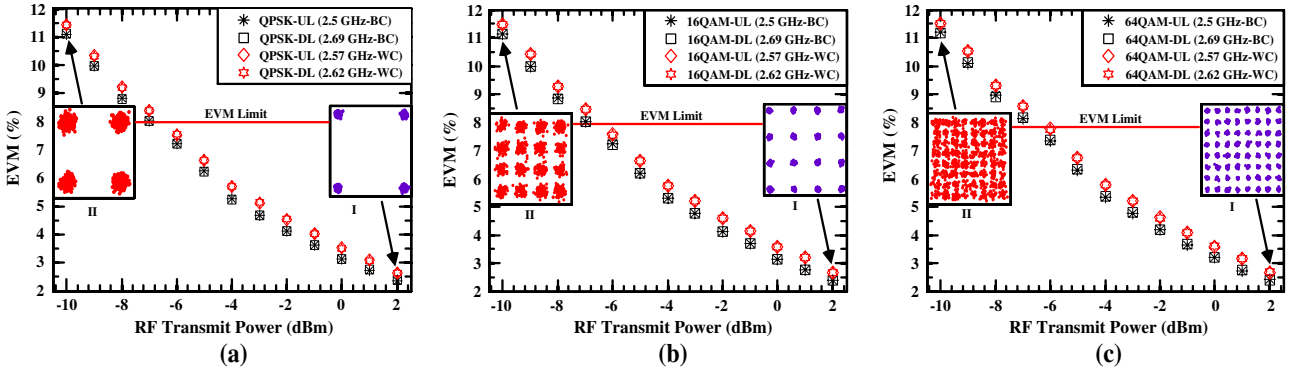

Fig. 10. EVM against RF transmit power for BC and WC transmission condition of (a) QPSK, (b) 16-QAM, and (c) 64-QAM. OLPs for all three modulation schemes are ∼1.06 dBm for DL and ∼1.19 dBm for UL.

Therefore, discussion on −10 dBm RF transmit power will not be carried out further for the subsequent modulations.

A similar degradation pattern of QPSK can be observed for 16-QAM and 64-QAM in Figs. 10(b) and 10(c), respectively. At 2 dBm transmit power, the best case and worst case transmission conditions EVMs for 16-QAM [Fig. 10(b)] are ∼2.33% and ∼2.61%, respectively. The corresponding constellation diagram for 2 dBm transmit power can be observed in inset I. For 64-QAM [Fig. 10(c)], the best case and worst case EVMs are ∼2.39% and ∼2.64%, respectively, while the constellation diagram can be observed in inset I. The average EVM deterioration observed for the worst case compared to the best case transmission condition is ∼0.36% across all three modulation schemes. The EVM deterioration reveals the robustness of the proposed system albeit using nonoptimal optical circulators. The overall system achieves an EVM below 8% with a transmit power as low as −6 dBm. Despite the variation in the constellation sizes between QPSK, 16-QAM, and 64-QAM, the EVMs achieved close proximity due to the normalization factor of the EVM relative to the individual constellation sizes; see Eq. (10) [32,34]. However, a larger constellation size requires a lower EVM to achieve the same bit error rate compared to a smaller constellation size [32,34].

It is also important to specify that the proposed system design does not include the short RF wireless link between the RN and UE, which will induce additional distortion. But since the highest RF transmit power of 2 dBm can achieve an EVM as low as ∼2.39% for a 64-QAM system, while the EVM limit for an LTE system is 8%, there is an additional error margin of 5.61% before the RF wireless link hits the limit. Furthermore, the system quality was demonstrated with a low EVM without the use of forward error correction, whereas in commercial systems, only coded modulation will be transmitted. Overall, the wireless link will not be a bottleneck for the proposed system.

V. Conclusion

In this paper, we have proposed the seamless integration of full duplex FDD LTE technology with AF RNs and a 10 km RoF system as the interface. The RoF system was designed based on dedicated directly modulated lasers for DL and UL with DWDM wavelength spacing and single SMF. The ACLR comparison between half duplex and full duplex systems with a BFS (190 MHz) revealed the system to be Rayleigh backscattering and optical interference free.

The DL system with BFS (190 MHz), IFS (120 MHz), and NFS (50 MHz) resulted in negligible, 0.69, and 14.10 dB ACLR penalties, respectively. In the UL system, the aforementioned frequency spacing achieved a close proximity to the DL system for the ACLR penalties. The BFS and IFS frequencies spacing experienced negligible IMD products. However, the NFS introduced severe IMD products from subcarrier–subcarrier intermixing due to the photodetection. Further studies on the interfering signal power were carried out with the aid of an ACLR and an EVM, where we found that the subcarrier–subcarrier intermixing effect is power dependent. In addition, we provided multiple EVM combinations for DL and UL signals with interfering UL and DL signals, respectively, within the range of 2 to −10 dBm RF transmit powers. Investigation showed that, irrespective of RF transmit power for the DL and UL signals, the average EVM deviation is ∼0.40% for the interfering UL and DL signals, within the maximum (2 dBm) and minimum (−10 dBm) RF transmit power.

Finally, we reported that the best case transmission condition for QPSK, 16-QAM, and 64-QAM systems achieved the average EVM values of ∼2.30%, ∼2.33%, and ∼2.39%, respectively, at 2 dBm transmit power.

References

[1] T. Wirth, L. Thiele, T. Haustein, O. Braz, and J. Stefanik, "LTE amplify and forward relaying for indoor coverage extension," in *IEEE 72nd Vehicular Technology Conf. Fall (VTC 2010-Fall)*, 2010, pp. 1–5.

[2] 3GPP, "3rd Generation Partnership Project; Technical Specification Group radio access network; evolved universal terrestrial radio access (E-UTRA) and evolved universal terrestrial radio access network (E-UTRAN)," 3GPP TS 36.300 V11.0.0, 2011.

[3] T. Wirth, V. Venkatkumar, T. Haustein, E. Schulz, and R. Halfmann, "LTE-advanced relaying for outdoor range extension," in *IEEE 70th Vehicular Technology Conf. Fall (VTC 2009-Fall)*, 2009, pp. 1–4.

[4] A. Nagate, K. Hoshino, M. Mikami, and T. Fujii, "A field trial of multi-cell cooperative transmission over LTE system," in *IEEE Int. Conf. on Communications (ICC)*, 2011, pp. 1–5.

[5] T. Kanesan, W. P. Ng, Z. Ghassemlooy, and J. Perez, "Optimization of optical modulator for LTE RoF in nonlinear fiber propagation," *IEEE Photon. Technol. Lett.*, vol. 24, pp. 617–619, 2012.

[6] W. P. Ng, T. Kanesan, Z. Ghassemlooy, and C. Lu, "Theoretical and experimental optimum system design for LTE-RoF over varying transmission span and identification of system nonlinear limit," *IEEE Photon. J.*, vol. 4, pp. 1560–1571, 2012.

[7] R. Letian, S. E. Elayoubi, and O. B. Haddada, "Impact of relays on LTE-advanced performance," in *IEEE Int. Conf. on Communications (ICC)*, 2010, pp. 1–6.

[8] P.-T. Shih, A. Ng'oma, C.-T. Lin, F. Annunziata, J. Chen, J. George, M. Sauer, and S. Chi, "2×21 Gbps symmetrical full-duplex transmission of OFDM wireless signals over a bidirectional IMDD radio-over-fiber system at 60 GHz," in *36th European Conf. and Exhibition on Optical Communication (ECOC)*, 2010, pp. 1–3.

[9] M. Milosavljevic, M. P. Thakur, P. Kourtessis, J. E. Mitchell, and J. M. Senior, "Demonstration of wireless backhauling over long-reach PONs," *J. Lightwave Technol.*, vol. 30, pp. 811–817, 2012.

[10] H.-C. Ji, K. Hoon, and C. C. Yun, "Full-duplex radio-over-fiber system using phase-modulated downlink and intensity-modulated uplink," *IEEE Photon. Technol. Lett.*, vol. 21, pp. 9–11, 2009.

[11] H.-J. Kim and J.-I. Song, "Full-duplex WDM-based RoF system using all-optical SSB frequency upconversion and wavelength re-use techniques," *IEEE Trans. Microwave Theory Tech.*, vol. 58, pp. 3175–3180, 2010.

[12] J. Yu, Z. Jia, T. Wang, and G. K. Chang, "Centralized lightwave radio-over-fiber system with photonic frequency quadrupling for high-frequency millimeter-wave generation," *IEEE Photon. Technol. Lett.*, vol. 19, pp. 1499–1501, 2007.

[13] M. Bakaul, A. Nirmalathas, and C. Lim, "Multifunctional WDM optical interface for millimeter-wave fiber-radio antenna base station," *J. Lightwave Technol.*, vol. 23, pp. 1210–1218, 2005.

[14] J. L. Wei, E. Hugues-Salas, R. P. Giddings, X. Q. Jin, X. Zheng, S. Mansoor, and J. M. Tang, "Wavelength reused bidirectional transmission of adaptively modulated optical OFDM signals in WDM-PONs incorporating SOA and RSOA intensity modulators," *Opt. Express*, vol. 18, pp. 9791–9808, 2010.

[15] C. Arellano, K. D. Langer, and J. Prat, "Reflections and multiple Rayleigh backscattering in WDM single-fiber loopback access networks," *J. Lightwave Technol.*, vol. 27, pp. 12–18, 2009.

[16] A. Chowdhury, H.-C. Chien, M.-F. Huang, J. Yu, and G.-K. Chang, "Rayleigh backscattering noise-eliminated 115-km long-reach bidirectional centralized WDM-PON with 10-Gb/s DPSK downstream and remodulated 2.5-Gb/s OCS-SCM upstream signal," *IEEE Photon. Technol. Lett.*, vol. 20, pp. 2081–2083, 2008.

[17] P. J. Winzer, F. Fidler, M. J. Matthews, L. E. Nelson, S. Chandrasekhar, L. L. Buhl, M. Winter, and D. Castagnozzi, "Electronic equalization and FEC enable bidirectional CWDM capacities of 9.6 Tb/s-km," in *Optical Fiber Communication Conf. (OFC)*, 2004, vol. 2, p. 3.

[18] J. Prat, V. Polo, C. Bock, C. Arellano, and J. J. V. Olmos, "Full-duplex single fiber transmission using FSK downstream and IM remote upstream modulations for fiber-to-the-home," *IEEE Photon. Technol. Lett.*, vol. 17, pp. 702–704, 2005.

[19] I. Papagiannakis, M. Omella, D. Klonidis, J. A. L. Villa, A. N. Birbas, J. Kikidis, I. Tomkos, and J. Prat, "Design characteristics for a full-duplex IM/IM bidirectional transmission at 10 Gb/s using low bandwidth RSOA," *J. Lightwave Technol.*, vol. 28, pp. 1094–1101, 2010.

[20] G. L. Li and P. K. L. Yu, "Optical intensity modulators for digital and analog applications," *J. Lightwave Technol.*, vol. 21, pp. 2010–2030, 2003.

[21] T. Kanesan, W. P. Ng, Z. Ghassemlooy, and C. Lu, "Impact of optical modulators in LTE RoF system with nonlinear compensator for enhanced power budget," in *Optical Fiber Communication Conf. and the Nat. Fiber Optic Engineers Conf. (OFC/NFOEC)*, 2013, pp. 1–3.

[22] 3GPP, "Evolved universal terrestrial radio access (E-UTRA); physical channels and modulation," 3GPP TS 36.211 V10.4.0, Rel-10, 2011.

[23] 3GPP, "Evolved universal terrestrial radio access (E-UTRA); user equipment (UE) radio transmission and reception," 3GPP TS 36.101 V10.4.0, Rel-10, 2011.

[24] X. Zheng, X. Q. Jin, R. P. Giddings, J. L. Wei, E. Hugues-Salas, Y. H. Hong, and J. M. Tang, "Negative power penalties of optical OFDM signal transmissions in directly modulated DFB laser-based IMDD systems incorporating negative dispersion fibers," *IEEE Photon. J.*, vol. 2, pp. 532–542, 2010.

[25] F. Ramos, J. Marti, V. Polo, and J. M. Fuster, "On the use of fiber-induced self-phase modulation to reduce chromatic dispersion effects in microwave/millimeter-wave optical systems," *IEEE Photon. Technol. Lett.*, vol. 10, pp. 1473–1475, 1998.

[26] R. Negi and J. Cioffi, "Pilot tone selection for channel estimation in a mobile OFDM system," *IEEE Trans. Consum. Electron.*, vol. 44, pp. 1122–1128, 1998.

[27] X. Zheng, J. L. Wei, and J. M. Tang, "Transmission performance of adaptively modulated optical OFDM modems using subcarrier modulation over SMF IMDD links for access and metropolitan area networks," *Opt. Express*, vol. 16, pp. 20427–20440, 2008.

[28] 3GPP, "Evolved universal terrestrial radio access (E-UTRA); base station (BS) radio transmission and reception," 3GPP TS 36.104 V9.1.0, Rel-9, 2010.

[29] C. Masse, "A 2.4 GHz direct conversion transmitter for Wimax applications," in *IEEE Radio Frequency Integrated Circuits (RFIC) Symp.*, 2006.

[30] L. Zhansheng, M. Sadeghi, G. de Valicourt, R. Brenot, and M. Violas, "Experimental validation of a reflective semiconductor optical amplifier model used as a modulator in radio over fiber systems," *IEEE Photon. Technol. Lett.*, vol. 23, pp. 576–578, 2011.

[31] D. Wake, A. Nkansah, N. J. Gomes, C. Lethien, C. Sion, and J. P. Vilcot, "Optically powered remote units for radio-over-fiber systems," *J. Lightwave Technol.*, vol. 26, pp. 2484–2491, 2008.

[32] R. Schmogrow, B. Nebendahl, M. Winter, A. Josten, D. Hillerkuss, S. Koenig, J. Meyer, M. Dreschmann, M. Huebner, C. Koos, J. Becker, W. Freude, and J. Leuthold, "Error vector magnitude as a performance measure for advanced modulation formats," *IEEE Photon. Technol. Lett.*, vol. 24, pp. 61–63, 2012.

[33] 3GPP, "LTE; evolved universal terrestrial radio access (E-UTRA); FDD repeater radio transmission and reception," 3GPP TS 36.106 V10.0.0, Rel-10, 2011.

[34] R. Bouziane, R. Koutsoyannis, P. Milder, Y. Benlachtar, J. C. Hoe, M. Glick, and R. I. Killey, "Optimizing FFT precision in optical OFDM transceivers," *IEEE Photon. Technol. Lett.*, vol. 23, pp. 1550–1552, 2011.